Electron emission in grazing-ion–surface collisions

M. S. Gravielle
Instituto de Astronomía y Física del Espacio, Casilla de Correo 67, Sucursal 28, 1428, Buenos Aires, Argentina
and Departamento de Física, Universidad Nacional de Buenos Aires, Buenos Aires, Argentina
(Received 19 May 2000; revised manuscript received 31 July 2000; published 14 November 2000)

For ions impinging grazingly on a solid surface, the electron emission from the inner shells of solid atoms is investigated by employing a semiclassical formalism. The emission rate is expressed in terms of probabilities of atomic ionization, which are evaluated with the continuum-distorted-wave–eikonal-initial-state approximation, taking into account the full dependency on the impact parameter. The model is applied to the calculation of the differential yield of ejected electrons for fast protons colliding with an aluminum surface. Inner-shell emission is compared with the electron emission from the valence band of the metal, considering different ejection angles. Calculated energy spectra of emitted electrons are in good agreement with the available experimental data.

PACS number(s): 34.50.Dy, 34.50.Bw

I. INTRODUCTION

The study of the angle and energy distributions of electrons emitted during the grazing scattering of fast ions from surfaces have been the subject of intense research during the last several years [1–11]. Its importance is based on the fact that electron emission produced in such ion-surface collisions carries information about the atomic and electronic structure of the topmost layer of the solid.

When a fast ion impinges on a metal surface with an incidence angle smaller than a given critical angle, the ion is specularly reflected from the surface without penetration inside the solid. For bare projectiles at high impact velocities, the charge state of the projectile can be considered as fixed [11–13], and the incident ion induces the emission of electrons from the solid. Ejected electrons may come from two different electronic sources of the metal: the valence band and the inner shells of target atoms. Both contributions can be calculated separately; while the valence-band ionization is expected to be dominant at large emission angles [14], the ionization from inner shells should play a prominent role for ejection angles close to the specular-reflection direction of the projectile [8].

The purpose of this work is to investigate the contribution of the ionization process from atomic inner shells to the energy spectrum of emitted electrons. We evaluate the inner-shell emission yield, also called the core contribution, by employing a semiclassical formalism in which the projectile trajectory is classically determined, while the electronic transitions are described with quantum methods. In the model the multiple collisions of the incident ion with the surface atoms are treated as single encounters with outermost atoms along the incoming and outgoing projectile paths. The emission probability per unit path is expressed in terms of atomic probabilities, which depend not only on the modulus of the impact parameter, but also on its direction. In the present work, the continuum-distorted-wave–eikonal-initial-state (CDW-EIS) approximation is used to calculate the impact-parameter-dependent probability of atomic ionization. This theory is a distorted-wave method that makes use of the eikonal wave function in the initial channel and the CDW wave function in the final channel. The CDW-EIS approximation has been found to be able to successfully explain the ionization process for a large variety of collision systems [15]. It takes into account the long-range behavior of the Coulomb potential, including the distortion produced by the projectile in both the initial and final channels.

We apply the theoretical model to the collision system composed of fast protons impinging grazingly on an aluminum surface, for which experimental data of electron emission have recently been published in Ref. [7]. With the aim of comparing the contributions of both electronic sources of the metal, the atomic inner shells and the valence band, when the ejection angle varies, we also calculate the emission from the valence band of the solid. In a previous paper [14] we have developed a semiclassical model to deal with binary collisions between the incident projectile and the electrons belonging to the free-electron gas. This model is here applied to the calculation of the rate of valence emission, using the first Born approximation to describe the electronic transitions. The plasmon decay mechanism is not included in the valence emission because it is expected that it contributes in the low-energy electron region [3,4,6], which is not considered in the present work. Finally, the energy spectrum of emitted electrons is studied in terms of the ejection angle, and the results are compared with the available experimental data [7].

The work is organized as follows. In Sec. II we introduce the theoretical model and the interaction potentials used to describe the core emission. Energy distributions for inner-shell emission are showed and discussed in Sec. III, comparing them with those originated by binary collisions with the valence band for different ejection angles. Section IV contains our conclusions. Atomic units are used unless otherwise stated.

II. THEORETICAL MODEL

A. Inner-shell emission

In this section we introduce the theoretical model employed to calculate the electron emission from the inner shells of target atoms. We consider a heavy projectile (P) of

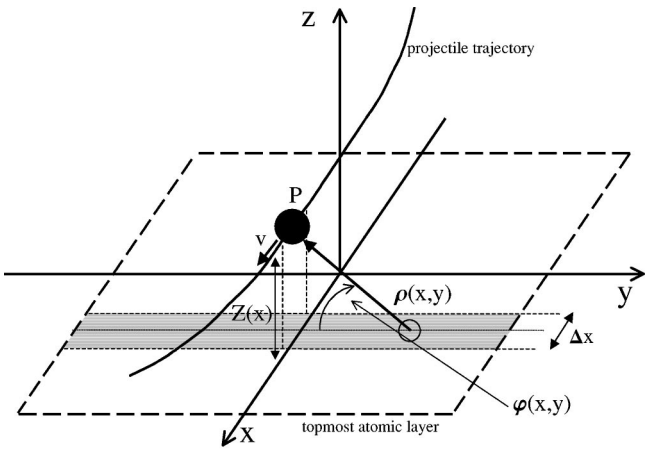

FIG. 1. Schematic picture of the coordinate system.

charge q and mass M_P impinging grazingly on a solid surface (S) of infinite mass. As a result of the collision, an electron (e) that it is initially bound to a target atom in the state i is emitted with momentum $\vec{k}_f$, which is measured in vacuum. Due to the large mass M_P of the projectile, the description of its motion in terms of a classical trajectory is a reasonable approximation. We use a frame of reference fixed to the position of the first atomic layer, with the projectile trajectory contained in the x-z plane, and the surface in the x-y plane (see Fig. 1). As a consequence of the symmetry of the problem, it is convenient to decompose the projectile velocity into two components: a two-dimensional vector parallel to the surface $\vec{v}_s$, and a component perpendicular to the surface v_z. In this way, we write the projectile velocity at the time t as $\vec{v}=(\vec{v}_s,v_z)=(v_s,0,v_z)$, and the initial impact velocity as $\vec{v}_i=(\vec{v}_{is},v_{iz})=(v_i\cos\theta_i,0,-v_i\sin\theta_i)$, θ_i being the angle of incidence defined with respect to the surface plane.

In grazing collisions the projectile trajectory can be divided in differential portions, with width Δx, situated at different distances $Z(x)$ from the surface. In every portion the component of the velocity perpendicular to the surface v_z is considered negligible, and the projectile moving parallel to the surface with velocity $\vec{v}_s$ induces the ejection of electrons from the inner shells of target atoms located in the corresponding surface band Δx. Since core electrons are strongly localized around atoms, only electrons of atoms situated at the first atomic plane contribute effectively to the electron emission [12]. Under those conditions transport effects are expected to play a minor role [10]. Therefore, ejected electrons can be considered as directly emitted to vacuum, without suffering multiple collisions with target nuclei. The emission probability per unit path, $dP_i(\vec{k}_f)/dx$, for the transition from the initial state i to the final state with momentum $\vec{k}_f$, is given by

$$\frac{dP_i(\vec{k}_f)}{dx}=\delta_S\int_{-\infty}^{+\infty}dy\,P_{i\,\vec{k}_f}^{(at)}(\vec{\rho}(x,y)), \tag{1}$$

where $P_{i\,\vec{k}_f}^{(at)}(\vec{\rho})$ is the probability of atomic ionization, depending on the impact-parameter $\vec{\rho}$, and δ_S is surface atomic density, which is considered as constant. In Eq. (1) the impact parameter depends on the position of the surface atom considered, with

$$\rho(x,y)=\sqrt{y^2+Z^2(x)},\quad \varphi(x,y)=\arctan\left(\frac{Z(x)}{y}\right), \tag{2}$$

the modulus and the azimuthal angle, respectively, of the impact parameter $\vec{\rho}(x,y)$ (see Fig. 1). The triple differential probability corresponding to the electronic transition $i\rightarrow\vec{k}_f$ is obtained by integrating $dP_i(\vec{k}_f)/dx$ along the projectile trajectory, and it reads

$$P_i(\vec{k}_f)\equiv d^3P_i/d\vec{k}_f=2\int_0^{+\infty}dx\,\frac{dP_i(\vec{k}_f)}{dx}, \tag{3}$$

where the factor 2 in front of the integral takes into account that the incoming and outgoing paths are equivalent.

In the present work, we employ the CDW-EIS approximation to evaluate the atomic probabilities $P_{i\,\vec{k}_f}^{(at)}(\vec{\rho})$. Assuming that the nonionized atomic electrons remains ''frozen'' during the collision, the problem is reduced to a one-active-electron system, and the T-matrix element reads

$$T_{i\,\vec{k}_f}^{CDW\text{-}EIS}=\langle\chi_f^{CDW}|W_f^{\dagger}|\chi_i^{E}\rangle, \tag{4}$$

where χ_f^{CDW} is the final CDW wave function, which contains a product of two continuum states, one around the target and the other around the projectile, χ_i^E is the eikonal wave function, and W_f is the final perturbative potential. In the CDW-EIS approximation the T-matrix element has a closed expression [16], and the atomic probability can be derived from Eq. (4) by using the well-known eikonal transformation $P_{i\,\vec{k}_f}^{(at)}(\vec{\rho})=|A_{i\,\vec{k}_f}^{CDW\text{-}EIS}(\vec{\rho})|^2$ [17], where

$$A_{i\,\vec{k}_f}^{CDW\text{-}EIS}(\vec{\rho})=\frac{2\pi}{v_s}\int d\vec{\eta}\,T_{i\,\vec{k}_f}^{CDW\text{-}EIS}\exp(i\vec{\eta}\cdot\vec{\rho}), \tag{5}$$

is the CDW-EIS transition amplitude, and $\vec{\eta}$ is the component of the transferred momentum perpendicular to $\vec{v}_s$.

The evaluation of $P_i(\vec{k}_f)$ involves a numerical four-dimensional integration. Calculations can be simplified if the dependence of atomic probability on the azimuthal angle φ is erased by averaging $P_{i\,\vec{k}_f}^{(at)}(\vec{\rho})$ over all different orientations of the impact parameter $\vec{\rho}$; that is

$$\mathcal{P}_{i\,\vec{k}_f}^{(at)}(\rho)=\frac{1}{2\pi}\int_0^{2\pi}d\varphi\,P_{i\,\vec{k}_f}^{(at)}(\vec{\rho}). \tag{6}$$

After replacing the average atomic probability $\mathcal{P}_{i\,\vec{k}_f}^{(at)}(\rho)$ in Eq. (1) and changing the integration variables, it leads to an approximate probability given by

$$\mathcal{P}_i(\vec{k}_f)=4\,\delta_S\int_{Z_0}^{+\infty}d\rho\,\rho\,\mathcal{P}_{i\,\vec{k}_f}^{(at)}(\rho)f(\rho), \tag{7}$$

where $f(\rho)=\int_{Z_0}^{\rho}dZ\,v_s v_z^{-1}(\rho^2-Z^2)^{-1/2}$ is a factor that only depends on the classical trajectory of the projectile, and Z_0 is the distance of the closest approach to the surface, with $Z_0>0$. In Sec. III we will investigate in detail the error introduced by approximating Eq. (3) by Eq. (7) (see Fig. 4).

B. Projectile trajectory

To calculate the emission probability $P_i(\vec{k}_f)$ it is necessary to know the classical trajectory of the projectile contained in Eq. (2). The projectile path $Z(x)$ is determined by the interaction $P-S$, which only depends on the distance to the surface plane. Therefore, the component of the projectile velocity parallel to the surface remains constant, i.e., $\vec{v}_s=\vec{v}_{is}$. The z component v_z satisfies the conservation of the energy in the perpendicular direction to the surface

$$\frac{1}{2}M_P v_{iz}^2=\frac{1}{2}M_P v_z^2+V_{PS}(Z), \tag{8}$$

where V_{PS} is the $P-S$ potential, and Z is the projectile distance to the topmost atomic layer. The classical path $Z(x)$ is derived from Eq. (8) by integrating the velocity $\vec{v}$ over the time, or equivalently, over the projectile position. Then, the trajectory equation reads

$$x=v_{is}\int_{Z_0}^{Z(x)}\left[v_{iz}^2-\frac{2}{M_P}V_{PS}(z')\right]^{-1/2}dz'. \tag{9}$$

The distance of the closest approach to the surface Z_0 is also calculated from Eq. (8) with the condition v_z tending to zero, i.e., $M_P v_{iz}^2/2=V_{PS}(Z_0)$.

The potential V_{PS} can be expressed as the sum of two interactions, $V_{PS}(Z)=V_{at}(Z)+V_{ind}(Z)$, where V_{at} is the static surface atomic potential, and V_{ind} is the induced electric potential. Both contributions originate by different mechanisms. The potential V_{at} is produced by the interaction of the projectile with the surface atoms, and it is here described by the usual Molière potential [18]. The potential V_{ind} corresponds to the induced field or dynamical image potential produced by the projectile moving close to the surface. We employ a simplified dielectric description given in Ref. [19] to represent V_{ind}, which reads

$$V_{ind}(Z)=-\frac{q^2 w_s^2}{2v_s w_s'}\int_0^{+\infty}d\xi\frac{\sin(\alpha\xi)}{(1+\xi^2)^{1/2}}\exp(-\beta\xi), \tag{10}$$

with $w_s'=(w_s^2-\gamma^2/4)^{1/2}$, where w_s is the surface plasma frequency and γ is the damping rate. The factors $\alpha=2w_s'Z/v_s$ and $\beta=\gamma Z/v_s$ are expressed in terms of the variable Z. The use of more sophisticated models to represent the potentials V_{at} and V_{ind} is not expected to introduce relevant differences in our results.

III. RESULTS

We confine our study to the collision system composed of fast protons impinging on an Al(111) surface with the angle of incidence $\theta_i=1°$, for which recent experimental data [7] are available. Two impact energies, 100 and 70 keV, are considered. At these energies protons can be considered as bare ions along the whole trajectory [20–22]; this system is then a good benchmark for the theory. The parameters used to describe the aluminum surface are the following. The interplanar separation is $d=4.4$ a.u., the Fermi energy is $E_F=0.414$ a.u. (the Fermi velocity $v_F=0.91$ a.u.), the work function is $E_W=0.15$ a.u., the surface plasma frequency is $w_s=0.4$ a.u., and $\gamma=0.037$ a.u. [19].

From Eq. (3) we calculate the inner-shell emission probability $P^{(is)}(\vec{k}_f)$ by adding over all occupied initial states, that is

$$P^{(is)}(\vec{k}_f)=\sum_i P_i(\vec{k}_f), \tag{11}$$

where the index i denotes the different atomic inner subshells. As the Al^0 contains three electrons in the outermost shell $n=3$, we consider that the target atoms cede these external electrons to the free-electron gas, keeping the rest of the electrons in the inner shells. In the present work, the atoms are considered as isolated and no correction is included to take into account that they are part of a surface. At the considered impact energies, the contribution coming from the K shell can be neglected in the calculation. This is a consequence of the slow projectile velocity in comparison with the mean orbital velocity of electrons in the $1s$ state. Then, only the initial states corresponding to the L shell of neutral aluminum are included in Eq. (11). The atomic bound states are described by Hartree-Fock double-z functions [23], and a Coulomb wave function with an effective charge satisfying the binding energy is employed to describe the final continuum state.

For every initial state, the evaluation of $P_i(\vec{k}_f)$ involves a double integral over the transferred momentum $\vec{\eta}$ as given by Eq. (5), and two other integrals on the surface plane (x,y). The integration on the variables $\vec{\eta}$ and y was numerically calculated with a relative error less than 3%, while the further integration on the variable x was solved by interpolating approximately 20 pivots, with the classical trajectory $Z(x)$ numerically obtained from Eq. (9).

In order to compare the electron emission originating from the different electronic sources of the metal, we also evaluate the emission probability of valence electrons $P^{(val)}(\vec{k}_f)$. Valence emission is due to collisions of the projectile with electrons of the free-electron gas, and it involves not only the binary mechanism but also collective effects. However, the collective contribution to the energy spectrum of the ejected electrons is expected to be important for electron energies around the value of the surface plasma frequency minus the work function, i.e., $w_s-E_W\approx 6.9$ eV [6]. Since such low-electron energies are not studied in the present work, the electron emission by plasmon decay will not be considered here.

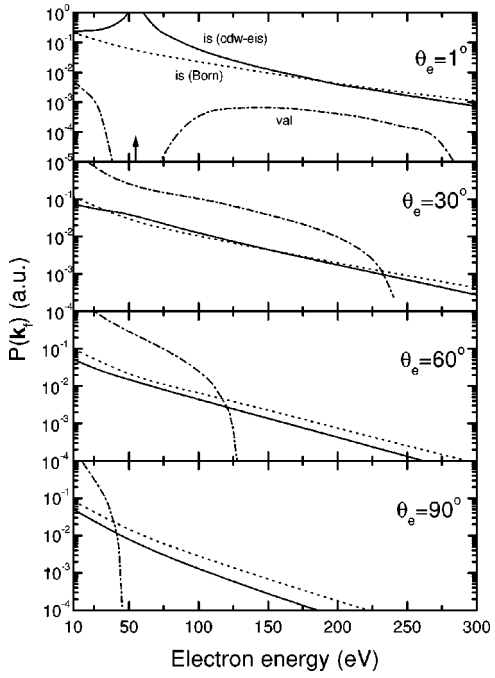

FIG. 2. Differential probability of the electron emission $P(\vec{k}_f) \equiv d^3P/d\vec{k}_f$ for 100-keV protons impinging on an Al(111) surface with the incidence angle $\theta_i = 1°$. Four ejection angles are considered: $\theta_e = 1°$, $\theta_e = 30°$, $\theta_e = 60°$, and $\theta_e = 90°$. Solid line, inner-shell emission probability $P^{(is)}(\vec{k}_f)$, calculated by using the CDW-EIS approximation; dotted line, inner-shell emission probability calculated with the first Born approximation; dashed-dotted line, valence emission probability $P^{(val)}(\vec{k}_f)$, calculated as explained in the text. The arrow indicates the position of the CTC peak.

We calculate the electron emission produced by binary collisions with the free-electron gas employing a semiclassical formalism developed in a previous paper [14]. In that model, the free-electron gas is described with the simple jellium model, the *T*-matrix element is evaluated with the first Born approximation, and a screened Coulomb potential is used to represent the interaction with the projectile. The differential emission probability $P^{(val)}(\vec{k}_f) \equiv d^3P^{(val)}/d\vec{k}_f$ is calculated from Eq. (12) of Ref. [14], using the same classical projectile trajectory that is used in the case of inner-shell ionization. Note that as the binary collisions with the free-electron gas satisfy the energy conservation (imposed by the δ function in Eq. (12) of Ref. [14]), the values of $\vec{k}_f$ reached with this mechanism are confined in the region

$$R_{\min} \leqslant |\vec{k}_f - \vec{v}_{is}| \leqslant R_{\max}, \tag{12}$$

with $R_{\max} = [(v_{is}+v_F)^2 - k_c^2]^{1/2}$ and $R_{\min} = [(v_{is}-v_F)^2 - k_c^2]^{1/2}$ $\Theta[v_{is} - (k_c + v_F)]$, where $k_c^2 = 2(E_F + E_W)$ and Θ is the unitary Heaviside function. Therefore, the binary electron emission from the valence band is only possible for values of v_{is} larger than $k_c - v_F$.

For 100-keV incident protons, in Fig. 2 we plot the inner-shell emission probability $P^{(is)}(\vec{k}_f)$ as a function of the electron energy, considering several ejection angles. The ejection angle θ_e is measured with respect to the surface plane. In this way, the final electron momentum outside the solid reads $\vec{k}_f = k_f$ (cos θ_e,0,sin θ_e), and $\epsilon_{\vec{k}_f} = k_f^2/2$ is the electron energy. The spectrum of core electrons is compared in Fig. 2 with that originating from the valence band for the different emission angles. While the valence electrons are emitted with energies localized in the range determined by Eq. (12), core emission is extended over the whole energy range considered, and tends to zero for high-electron energies when the angle θ_e increases. At the angle $\theta_e = 1°$, which coincides with the direction of the outgoing projectile, the core emission is almost two orders of magnitude higher than the valence emission for the lower-electron energies. In the forward direction the probability $P^{(is)}(\vec{k}_f)$ shows a peak at $\epsilon_{\vec{k}_f} \simeq v_{is}^2/2$, which corresponds to the well-known capture to the continuum (CTC) peak, convoluted by the surface symmetry. Precisely, for electron energies around the CTC peak, the ejection of valence electrons is not possible by binary collisions, and multiple-scattering processes have been found quite unlikely [8]. For reference, in Fig. 2 we also plot the Born probability of inner-shell emission. This probability is derived from Eq. (1) by using the first Born approximation, instead of the CDW-EIS approximation, to evaluate the atomic ionization probability. At the ejection angle $\theta_e = 1°$ the Born probability does not display the structure corresponding to the CTC peak, and it tends to the results of the CDW-EIS approximation for high-electron energies, as typical in atomic collisions [15].

From Fig. 2 we observe that when the ejection angle increases (separating from the direction of specular reflection of the projectile) the binary emission from the valence band gives the more important contribution at low-electron energies. However, the range of electron energies reached with this mechanism diminishes abruptly for large values of θ_e, and the spectrum of fast electrons is dominated by core emission. For $\theta_e = 30°$ the Born probability coincides with results of the CDW-EIS approximation, but it runs above the CDW-EIS curve for larger angles. Another important feature of the spectrum of ejected electrons is the absence of the binary peak in the inner-shell emission probability. The binary peak is missing in the core spectrum because the projectile velocity is lower than the orbital velocity of bound electrons. On the contrary, this peak appears clearly in the valence emission probability, and its width is due to the initial momentum distribution of electrons of the free-electron gas, as can be observed from Eq. (12) [8].

Contributions of the different subshells to the emission spectrum are displayed in Fig. 3 for the same ejection angles considered in Fig. 2, i.e., $\theta_e = 1°$, 30°, 60°, and 90°. In the forward direction $\theta_e = 1°$, the ejection of slow electrons is dominated by the ionization from the $2p_0$ state, while contributions from $2p_{\pm 1}$ states are higher for high electron energies. Notice that in the energy region around the CTC peak, all subshells contribute to the emission probability. At $\theta_e = 30°$ the situation is inverse: contributions from the $2p_{\pm 1}$ states are higher at low-electron energies, while the emission from the $2p_0$ state dominates at high energies. For both angles, $\theta_e = 1°$ and $\theta_e = 30°$, the probability of emission

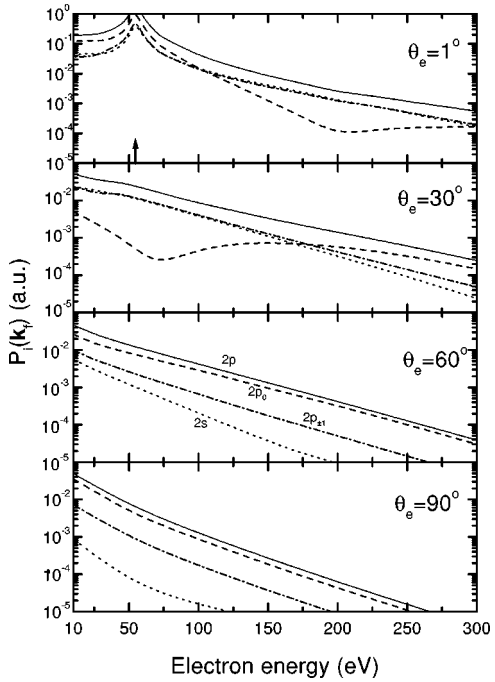

FIG. 3. Partial contributions to the inner-shell emission for 100-keV protons impinging on an Al(111) surface with the incidence angle $\theta_i = 1°$ for different ejection angles θ_e. Ionization from the $2p$ orbital (thin solid line), the $2p_0$ orbital (dashed line), the $2p_{\pm 1}$ orbital (dashed-dotted line), and the $2s$ orbital (dotted line) of Al^0. The arrow indicates the position of the CTC peak.

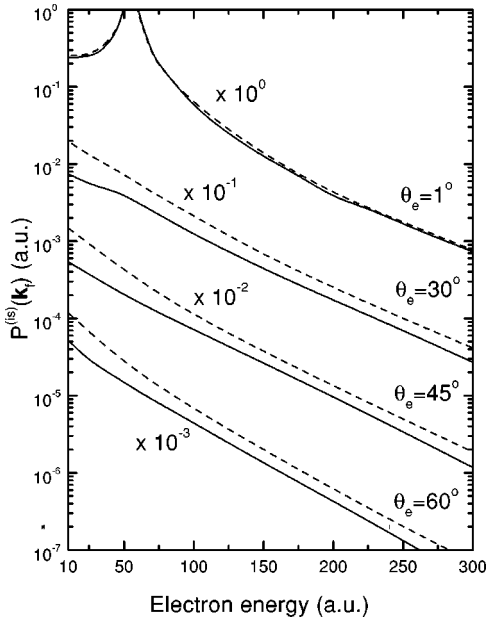

FIG. 4. Differential probability of the inner-shell emission for 100-keV protons impinging on an Al(111) surface with the incidence angle $\theta_i = 1°$ for different ejection angles θ_e. Solid line, probability derived from Eq. (3), taking into account the full dependency on the azimuthal angle φ; dashed line, approximated probability derived from Eq. (7) by averaging the φ dependency of the atomic probability; both probabilities calculated with the CDW-EIS approximation.

from the $2s$ state runs close to the one from the $2p_{\pm 1}$ states for all the electron energies considered. For larger emission angles, $\theta_e = 60°$ and $90°$, the electrons are ejected preferentially from the $2p_0$ state, and the $2s$ contribution is one and two orders of magnitude smaller, respectively.

To investigate the error that it is introduced by averaging the dependency on orientation of the impact parameter in the atomic probability, in Fig. 4 we compare the emission probability $P^{(is)}(\vec{k}_f)$ obtained from Eq. (3) with the approximated value $\mathcal{P}^{(is)}(\vec{k}_f)$ derived from Eq. (7), for 100-keV impact energy and different ejection angles. In the forward direction, $\mathcal{P}^{(is)}(\vec{k}_f)$ runs joined with the values of $P^{(is)}(\vec{k}_f)$, while for other angles it detaches from the exact curve, running above $P^{(is)}(\vec{k}_f)$ by a factor ranging from 1.4 to 3.0. Notice that although averaging of the angle φ produces non-negligible effects in the core emission spectrum for intermediate angles, it weakly affects the total rate of inner-shell emission, as proposed by other authors [12].

Finally, we study the total binary contribution to the energy spectrum of emitted electrons in terms of the ejection angle. The emission probability $P(\vec{k}_f) \equiv d^3P/d\vec{k}_f$ is defined as the sum of the partial probabilities coming from both core and valence electrons; that is

$$P(\vec{k}_f) = P^{(is)}(\vec{k}_f) + P^{(val)}(\vec{k}_f). \tag{13}$$

In Fig. 5 results for 100-keV protons are compared with the experimental data of Ref. [7], normalized by using our theoretical values for the electron energy of 200 eV. Although this electron energy is arbitrarily chosen, the value of the normalization factor does not change appreciably for electron energies between 125 and 200 eV. The partial contributions $P^{(is)}(\vec{k}_f)$ and $P^{(val)}(\vec{k}_f)$ are also plotted in Fig. 5, displaying the electron energy ranges where each mechanism is dominant. Emission probabilities obtained from Eq. (13) show a good agreement with the experiments, in particular for the ejection angle coinciding with the exit direction of the projectile. For larger angles, the discrepancy observed at high electron energies may be caused by the emission of energetic valence electrons as a consequence of multiple-scattering processes, which are not included in our formalism [8].

With the aim of studying the inner-shell contribution around the CTC peak when the impact velocity varies, in Fig. 6 we plot the emission probability at $\theta_e = 1°$ for 70-keV protons. This impact energy corresponds to the lowest velocity limit that could be dealt with our model. As in Fig. 5, partial contributions of core and valence electrons are also displayed. In the forward direction, inner-shell emission gives again the most important contribution over the whole electron energy range. Around the CTC peak, the ejection of valence electrons by binary collisions is two orders of magnitude smaller than the core emission. Total emission probability $P(\vec{k}_f)$ is compared with the experimental data of Ref. [7], normalized with our theoretical value for the electron energy of 130 eV. In this case, the normalization factor dramatically depends on the chosen electron energy. Note our

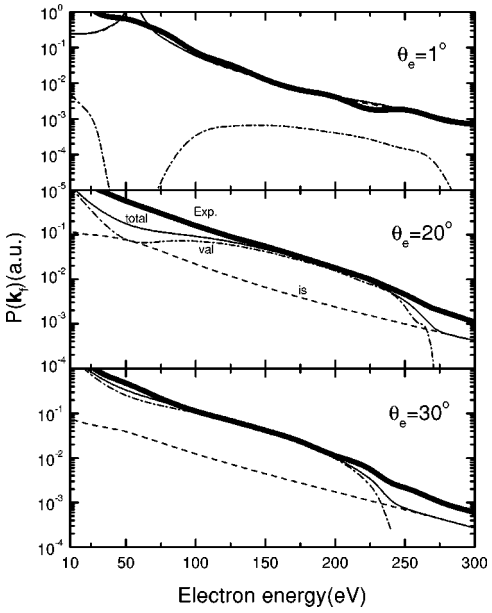

FIG. 5. Differential probability of the electron emission $P(\vec{k}_f) \equiv d^3P/d\vec{k}_f$ for 100-keV protons impinging on an Al(111) surface with the incidence angle $\theta_i = 1°$. Three electron emission angles are considered: $\theta_e = 1°$, $\theta_e = 20°$, and $\theta_e = 30°$. Solid line, total probability of emission by binary collisions, calculated from Eq. (13); dashed line, inner-shell contribution $P^{(is)}(\vec{k}_f)$; and dashed-dotted line, valence contribution $P^{(val)}(\vec{k}_f)$. The thick solid line represents experimental data extracted from Ref. [7], normalized with our theoretical values, as explained in the text.

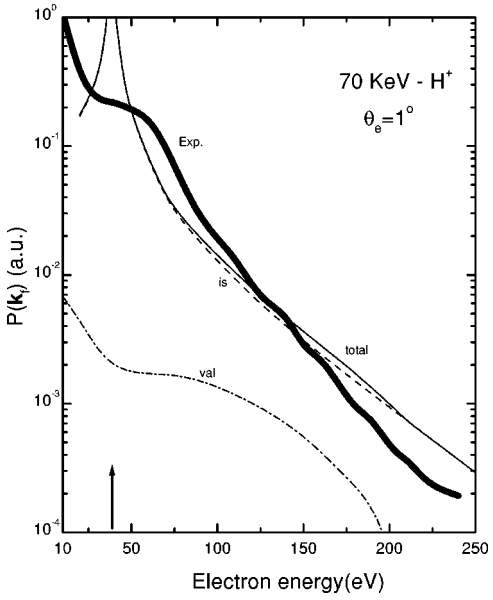

FIG. 6. Differential probability of the electron emission $P(\vec{k}_f) \equiv d^3P/d\vec{k}_f$ for 70-keV protons impinging on an Al(111) surface with the incidence angle $\theta_i = 1°$, at the emission angle $\theta_e = 1°$. Theory and experiment as in Fig. 5. The arrow indicates the position of the CTC peak.

results have not been corrected by the transmission function of the experimental analyzer. The agreement with the experiments is qualitatively good around the CTC peak, but theoretical and experimental curves show different slopes when the electron energy increases. Since the CDW-EIS approximation is a high-energy method, measurements for higher impact velocities would be desirable to test the model.

IV. CONCLUSIONS

We have presented a semiclassical theory to deal with electron emission from the inner shells of solid atoms, originated by ion-surface scattering. The theory describes the multiple collisions of the projectile with the surface atoms along the trajectory, being only valid for grazing impact. In the model the emission rate is expressed in terms of probabilities of atomic ionization, taking into account the full dependency on the impact parameter. To evaluate atomic probabilities we employed the CDW-EIS approximation, which is valid in the high-velocity region. The formalism is applied to the calculation of energy spectra of ejected electrons for fast protons impinging grazingly on an aluminum surface, for which there are recent experimental results [7]. The core emission is compared with the electron emission from the valence band, considering different ejection angles. The ionization of valence electrons is calculated with a method derived in Ref. [14] which describes the binary collisions with the free-electron gas. Partial contributions originated by ionization from different atomic subshells are analyzed. For the ejection angle coincident with the specular-reflection direction of the projectile, the ionization from the inner shells represents the dominant mechanism while the valence-band ionization prevails at low-electron energies for large ejection angles. Differential probability of electron emission from both atomic inner shells and the valence band shows a good agreement with the available experimental data for 100-keV protons. The method employed to calculate the valence emission is only valid to deal with metals or semiconductors with a small gap. Instead, the proposed theoretical model is expected to also be successful in dealing inner-shell emission from metal and nonmetal surfaces.

ACKNOWLEDGMENTS

The author gratefully acknowledges useful and stimulating discussions with J. E. Miraglia.

[1] K. Kimura, M. Tsuji, and M. Mannami, Phys. Rev. A **46**, 2618 (1992).
[2] U. Thumm, J. Phys. B **25**, 421 (1992).
[3] D.L. Mills, Surf. Sci. **294**, 161 (1993).
[4] F.J. García de Abajo and P.M. Echenique, Nucl. Instrum. Methods Phys. Res. B **79**, 15 (1993).
[5] E.A. Sánchez, O. Grizzi, M.L. Martiarena, and V.H. Ponce, Phys. Rev. Lett. **71**, 801 (1993).

[6] F.J. Garcí a de Abajo, Nucl. Instrum. Methods Phys. Res. B **98**, 445 (1995).
[7] M.L. Martiarena, E.A. Sánchez, O. Grizzi, and V.H. Ponce, Phys. Rev. A **53**, 895 (1996).
[8] C.O. Reinhold and J. Burgdörfer, Phys. Rev. A **55**, 450 (1997).
[9] R. Minniti, S.B. Elston, C.O. Reinhold, J.Y. Lim, and J. Burgdörfer, Phys. Rev. A **57**, 2731 (1998).
[10] K. Kimura, S. Ooki, G. Andou, K. Nakajima, and M. Mannami, Phys. Rev. A **58**, 1282 (1998).
[11] K. Kimura, S. Ooki, G. Andou, and K. Nakajima, Phys. Rev. A **61**, 012901 (2000).
[12] J.I. Juaristi, F.J. García de Abajo, and P.M. Echenique, Phys. Rev. B **53**, 13 839 (1996).
[13] C.C. Montanari, M.S. Gravielle, V.D. Rodríguez, and J.E. Miraglia, Phys. Rev. A **61**, 022901 (2000).
[14] M.S. Gravielle, Phys. Rev. A **58**, 4622 (1998).
[15] P.D. Fainstein, V.H. Ponce, and R.D. Rivarola, J. Phys. B **24**, 3091 (1991).
[16] P.D. Fainstein, V.H. Ponce, and R.D. Rivarola, J. Phys. B **22**, 1207 (1989).
[17] M.R.C. McDowell and J.P.Coleman, *Introduction to the Theory of Ion-Atom Collisions* (North-Holland, Amsterdam, 1970).
[18] V.G. Molière, Z. Naturforsch **2**, 133 (1947).
[19] N.R. Arista, Phys. Rev. A **49**, 1885 (1994).
[20] H. Winter, R. Kirsch, J.C. Poizat, and J. Remillieux, Phys. Rev. A **43**, 1660 (1991).
[21] J.E. Miraglia, Phys. Rev. A **50**, 2410 (1994).
[22] M.S. Gravielle and J.E. Miraglia, Phys. Rev. A **50**, 2425 (1994); **50**, 3202 (1994).
[23] E. Clementi and C. Roetti, At. Data Nucl. Data Tables **14**, 177 (1974), Table 42.